Ionics (2020) 26:2655–2664
https://doi.org/10.1007/s11581-019-03403-9

ORIGINAL PAPER

Effect of Nb^{5+} doping on $LiNi_{0.5}Co_{0.25}Mn_{0.25}O_2$ cathode material

Lina Li[1] · Enshan Han[1] · Lingzhi Zhu[1] · Shunpan Qiao[1] · Chenyu Du[1]

Received: 11 October 2019 / Revised: 6 December 2019 / Accepted: 12 December 2019 / Published online: 2 January 2020

Abstract

Li $(Ni_{0.5}Co_{0.25}Mn_{0.25})_{1-x}Nb_xO_2$ ($x = 0$, 0.005, 0.01, 0.02, 0.03) cathode material was synthesized by co-precipitation. X-ray diffraction spectroscopy (XRD) and scanning electron microscopy (SEM) were used to analyze the crystal structure characteristics and morphology of the powder. The charge and discharge test, electrochemical impedance spectroscopy (EIS), and cyclic voltammetry (CV) were used to study the electrochemical properties of the battery in detail. XRD results show that Nb^{5+} substitution does not destroy the crystal structure, but it can enlarge the interplanar spacing, which is beneficial to the diffusion of lithium ions. The electrochemical properties of the material Li $(Ni_{0.5}Co_{0.25}Mn_{0.25})_{0.99}Nb_{0.01}O_2$ are the best. The discharge specific capacity is 204.6, 186.0, 163.5, 141.6 mAh/g at 0.1C, 0.2C, 0.5C, and 1.0C, respectively. And the discharge specific capacity is as high as 174.1 mAh/g when returning to 0.1C again. After circulating 45 cycles at 0.1C, the capacity retention rate was 89.08%.

Keywords Cathode material · Nb^{5+} substitution · Electrochemical properties

Introduction

With the development of electric vehicles, large-scale electronic equipment, and hybrid vehicles, lithium-ion batteries have received extensive attention [1]. Lithium-ion batteries have enormous global potential for achieving energy sustainability and significantly reducing carbon emissions [2]. The requirements for lithium-ion batteries are increasing, such as high energy density, excellent cycle stability, and reliable safety [3, 4]. Lithium-ion batteries of widely used $LiCoO_2$ materials are hexagonal α-$NaFeO_2$-type belonging to the R-3m space group. This layered structure allows $LiCoO_2$ to have good lithium-ion intercalation/deintercalation capabilities. However, the structural stability of $LiCoO_2$ deteriorates drastically when lithium ions are half-extracted from the structure during charging. Therefore, in order to ensure its cycle performance limits its cut-off voltage, it can only provide half of the theoretical capacity of about 140 mAh/g capacity [5, 6]. The ternary cathode material $LiNi_{1-x-y}Co_xMn_yO_2$ has a structure similar to $LiCoO_2$, and because it has the advantages of relatively low cost, high capacity, and better thermal stability, it can be used instead of $LiCoO_2$ [7, 8]. However, studies have shown that $LiNi_{1-x-y}Co_xMn_yO_2$ ($0 < x < 1$, $0 < y < 1$ $x + y = 1$) has a faster capacity loss. It is because of stone and rock salt phase transition due to Ni^{2+} being more likely to occupy the Li^+ position [9–12], oxygen in the lattice released from the surface [3, 13, 14], and other shortcomings resulting in poor crystal structure [15].

In order to improve the performance of lithium-ion batteries, people mainly study cathode materials and electrolytes [16, 17]. The main modification methods for lithium-ion ternary cathode materials are doping [18–20], coating [21, 22], and core-shell structure [23].

The method of element doping refers to doping with other small amounts of metal or non-metal elements inside the crystal lattice, and it is desirable to improve certain electrochemical properties of the original material. The radius of Nb^{5+} is 0.064 nm, and the radius of Mn^{4+} is 0.053 nm. Since the radius of Nb^{5+} is close to the radius of the transition element and Nb^{5+} has a larger diameter than Mn^{4+} [24], Nb^{5+} can enhance the lattice parameters. It is important that it has a higher metal-oxygen bond energy. Hu et al. studied the effect of Nb doping on the positive electrode material $0.5Li_2MnO_3 \cdot 0.5LiNi_{1/3}Co_{1/3}Mn_{1/3}O_2$, and found that Nb is most effective in improving cycle performance and reducing voltage attenuation [25]. Yi et al. performed Nb doping on $LiMn_2O_4$. The results show that Nb doping can reduce electrode polarization and increase lithium-ion diffusion coefficient [26].

✉ Enshan Han
eshan@hebut.edu.cn

[1] School of Chemical Engineering and Technology, Hebei University of Technology, Tianjin 300130, People's Republic of China

Considering the substitution of Nb^{5+} may improve the electrochemical properties of the material $LiNi_{0.5}Co_{0.25}Mn_{0.25}O_2$ in some extent. In this paper, we prepared Li $(Ni_{0.5}Co_{0.25}Mn_{0.25})_{1-x}Nb_xO_2$ ($x = 0$, 0.005, 0.01, 0.02, 0.03) by co-precipitation. The effects of Nb^{5+} doping on the structure, morphology, and electrochemical properties of the cathode material $LiNi_{0.5}Co_{0.25}Mn_{0.25}O_2$ were investigated in detail.

Experiment

Synthesis

The precursor $Ni_{0.5}Co_{0.25}Mn_{0.25}(OH)_2$ was first prepared by hydroxide coprecipitation, and then Nb^{5+} was introduced in the ball milling stage. The mixture which was composed of $NiSO_4·6H_2O$, $CoSO_4·7H_2O$, and $MnSO_4·H_2O$ in a molar ratio of 5:2.5:2.5 was dissolved in a small amount of deionized water and then configured as a solution having a transition metal ion concentration of 1 mol/L. The precipitant NaOH solution was prepared to be 2 mol/L, and the complexing agent $NH_3·H_2O$ was set to 1 mol/L. The three solutions were simultaneously pumped into the reactor while maintaining a reaction temperature of 55 °C and a pH of 11. After the reaction was completed, the mixture was stirred at a constant temperature for 2 h, and finally it was aged overnight. The suspension was thoroughly washed and filtered to remove impurity ions (Na^+, SO_4^{2+}, NH_3^+, etc.). After the end of the suction filtration, the filter cake was placed in a blast drying oven at 102 °C to remove moisture.

According to the stoichiometric molar ratio of the chemical formula Li $(Ni_{0.5}Co_{0.25}Mn_{0.25})_{1-x}Nb_xO_2$ ($x = 0$, 0.005, 0.01, 0.02, 0.03), the prepared powder was ball milled with Li_2CO_3 and Nb_2O_5, and the amount of Li_2CO_3 added was 5% higher than the calculated value, and Nb_2O_5 was used as the niobium source. The milling time is 5 h to make them mix uniformly.

The resulting mixture was placed in a muffle furnace and heated to 450 °C at a heating rate of 5 °C/min in an oxygen atmosphere, and then preheated for 5 h. After cooling to room temperature in a furnace, it was taken out and carefully ground. Finally, the temperature was raised to 850 °C at a heating rate of 5 °C/min, and the ground powder was calcined at 850 °C for 12 h to obtain a final product.

Electrode film and battery assembly preparation

First, the active material, acetylene black, and PVDF (polyvinylidene fluoride) were in an amount of 8:1:1, and the NMP (N-methyl-pyrrolidone) was taken in an appropriate amount. Acetylene black was added as a conductive agent, and PVDF was used as a binder. The active material and acetylene black were thoroughly ground in an agate mortar, and then PVDF was dissolved in NMP. The ground mixture was added to the solution. Stirring was carried out to obtain a uniformly dispersed slurry, which was then uniformly coated on an aluminum foil. The coated aluminum foil was dried at 110 °C for 10 h. After drying, it was compacted by a tableting machine and then punched into circular electrode sheets having a diameter of 10 mm.

Second, the preparation of the battery assembly was carried out in a dry inert gas glove box. The operation sequence was first placed with a negative electrode (lithium plate), a separator (Celgard 2400 porous polypropylene film), an appropriate amount of electrolyte 1 mol/L $LiPF_6$ (EC+EMC+DMC

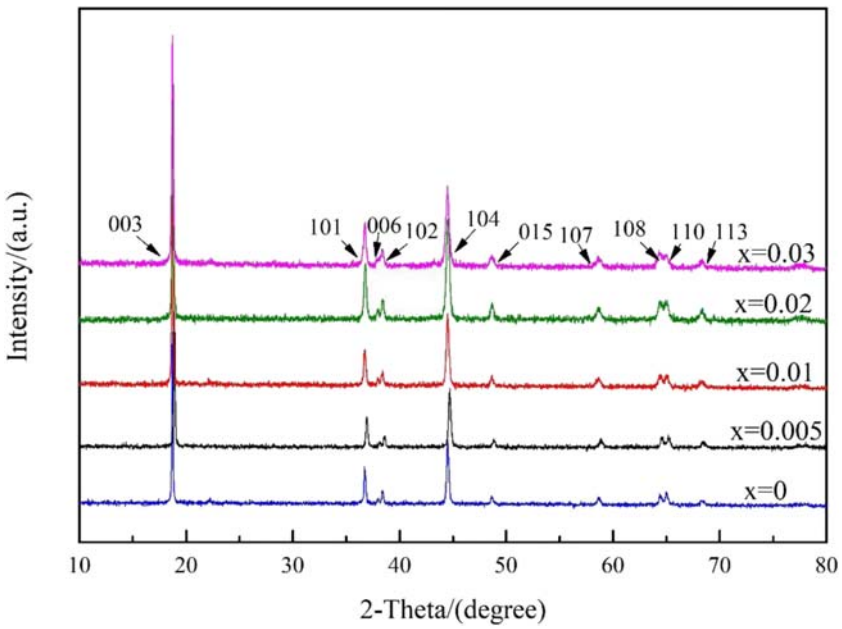

Fig. 1 XRD pattern of Li $(Ni_{0.5}Co_{0.25}Mn_{0.25})_{1-x}Nb_xO_2$

Table 1 Lattice parameters of Li $(Ni_{0.5}Co_{0.25}Mn_{0.25})_{1-x}Nb_xO_2$

Samples	a	b	c	c/a	V(Å)	$R(I_{003}/I_{104})$
$x = 0$	2.86024	2.86024	14.18125	4.95806	100.47	1.617
$x = 0.005$	2.86309	2.86309	14.19739	4.95876	100.79	1.812
$x = 0.01$	2.86725	2.86725	14.22851	4.96242	101.30	2.208
$x = 0.02$	2.86755	2.86755	14.23122	4.96284	101.34	2.175
$x = 0.03$	2.86690	2.86690	14.25015	4.97058	101.43	2.494

volume ratio 1:1:1), and a positive electrode sheet. It was sealed and subjected to electrochemical test after standing for 24 h.

Physical characterization and electrochemical performance of materials

The crystal structure was analyzed using an X-ray diffraction analyzer ((XRD), Bruke D8-Fouse, Germany) which uses Cu-Kα as a radiation source with a scanning range of $2\theta = 10$–$80°$ and a scanning speed of 12°/min. The morphology of the synthesized powder was analyzed by scanning electron microscopy ((SEM), Nova Nano SEM450 FEI), and energy dispersive spectrometer ((EDS), manufactured by AMETEK, model OCTANE PLUS) was used to test the element content in the material. The surface chemical compositions of the samples were measured by X-ray photoelectron spectroscopy ((XPS), ESCALAB 250Xi).

Charge and discharge were tested by the battery test system Land CT2001A with a test voltage range of 2.7–4.3 V. Both cyclic voltammetry (CV) and electrochemical impedance spectroscopy (EIS) were tested on PARSTAT 4000 electrochemical analyzer. The test parameters for CV were a scan rate of 0.1 mV/s and a voltage range of 2.7–4.5 V. The EIS test amplitude is 5 mV in the frequency range of 100 kHz to 0.01 Hz. The EIS data was analyzed using the ZsimpWin 3.10 software. All the characterizations and measurements were taken at room temperature.

Results and discussion

Physical characterization

Figure 1 shows the XRD pattern of Li $(Ni_{0.5}Co_{0.25}Mn_{0.25})_{1-x}Nb_xO_2$, all of which are consistent with the layered features of α-$NaFeO_2$. Compared with the undoped material, it is found that the position of the Nb^{5+} doped material peak does

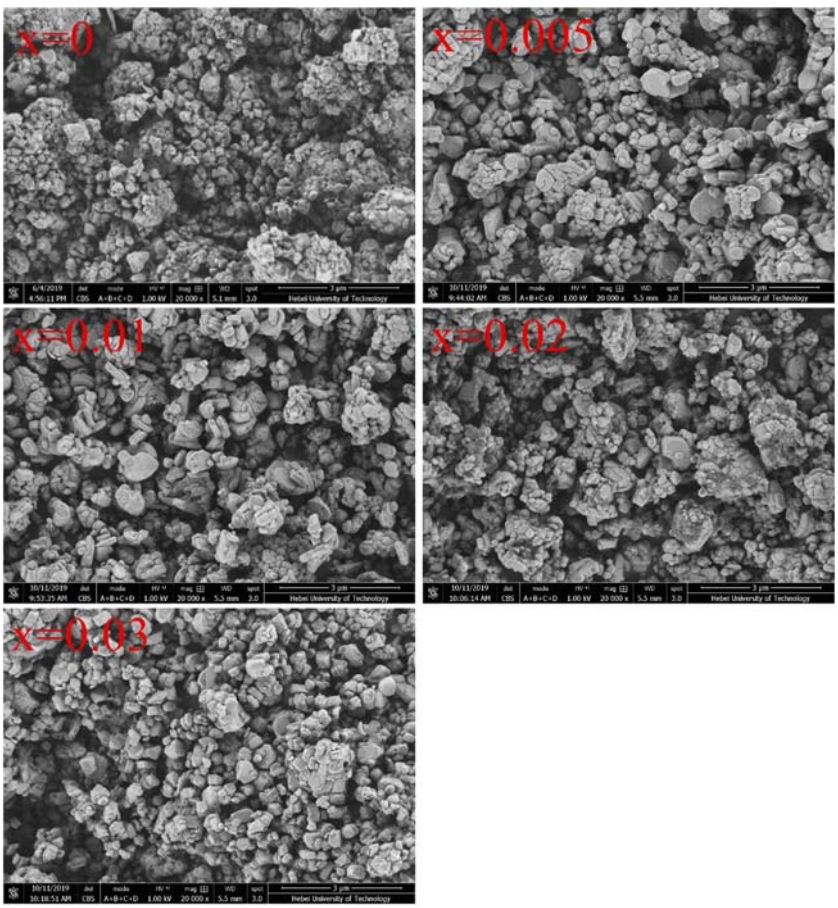

Fig. 2 SEM image of Li $(Ni_{0.5}Co_{0.25}Mn_{0.25})_{1-x}Nb_xO_2$

not change. Each peak has a characteristic peak of a typical α-$NaFeO_2$ structure, and the shape of the peak is clear, and the intensity is large. This indicates that Nb^{5+} doping does not change the crystal structure of the original material. By carefully comparing the samples $x = 0$, $x = 0.005$, $x = 0.01$, $x = 0.02$, $x = 0.03$, it is found that the (006)/(102) peak is equally sharp except for sample $x = 0.03$. The (108)/(110) peaks all have good splitting, indicating a layered structure. Table 1 summarizes the unit cell parameters after refining of all samples. As the Nb^{5+} doping content increases, the lattice

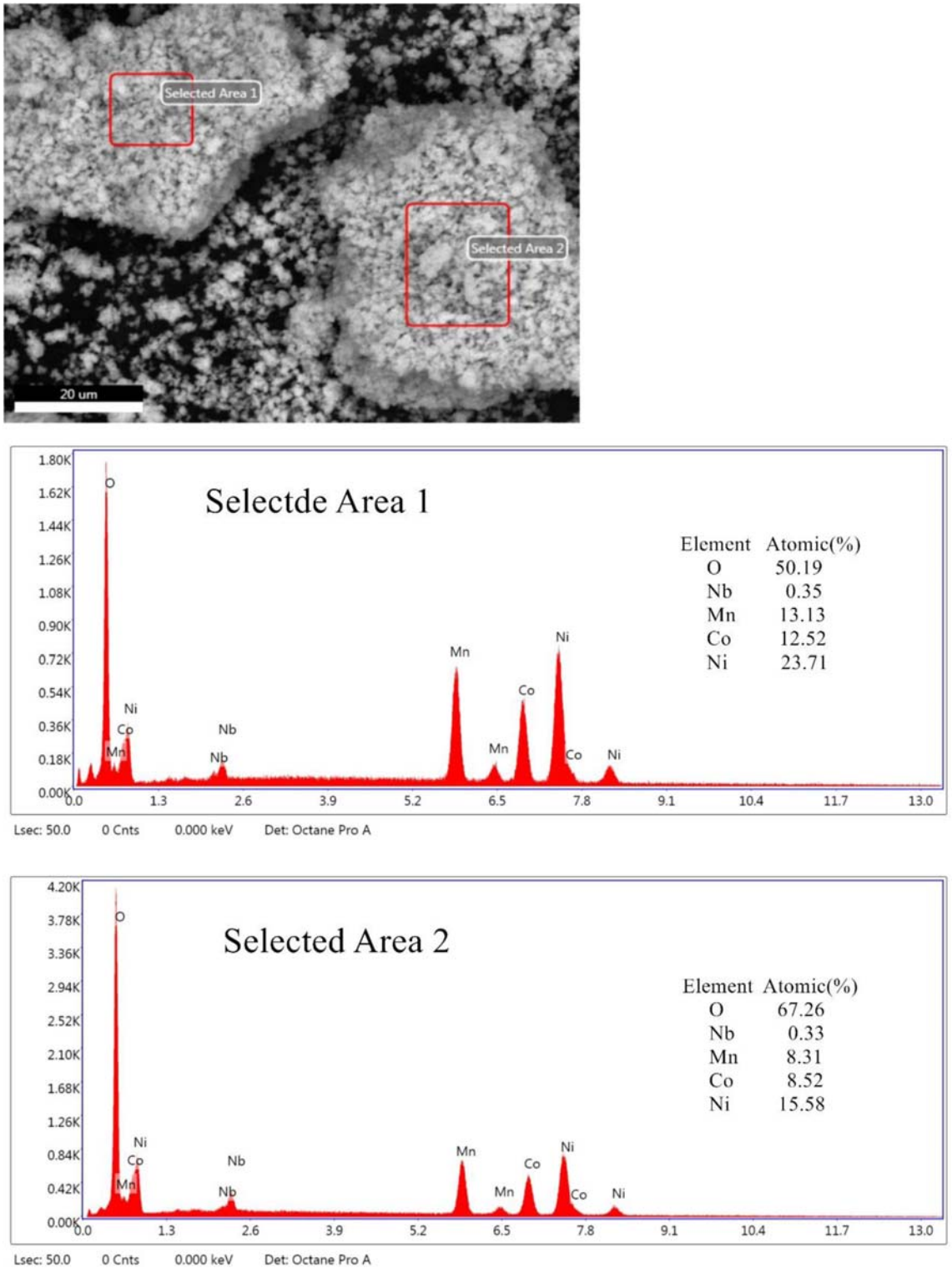

Fig. 3 EDS image of Li $(Ni_{0.5}Co_{0.25}Mn_{0.25})_{0.99}Nb_{0.01}O_2$

parameters a and c show a slight increase, indicating that the modification has induced the structure [27]. It can be seen from the volume parameter that the lattice volume after doping is larger than the original one. This may be due to the ionic radius of Nb^{5+} (0.64 Å) being larger than that of Mn^{4+} (0.53 Å) [24]. After doping, the intensity ratio of I(003)/I(104) are all larger than the original intensity ratio, which indicates that Li^{+}/Ni^{2+} mixing is reduced [25].

In order to observe the surface topography of the material, Fig. 2 was obtained by scanning electron microscope. It can be seen that the Li $(Ni_{0.5}Co_{0.25}Mn_{0.25})_{1-x}Nb_xO_2$ particles consist of densely packed particles. The microspherical particles can effectively shorten the Li^{+} diffusion path, reduce volume expansion/compression during charging/discharging, and promote diffusion of electrolyte into the electrode material [28]. The particle surface of Li $(Ni_{0.5}Co_{0.25}Mn_{0.25})_{0.99}Nb_{0.01}O_2$ material is very smooth and clean. Its particle size is the most uniform, so its electrochemical performance should be the best.

In order to determine the elemental composition and distribution of the sample, and further prove the uniformity of Nb^{5+} doping, EDS spectrum testing was performed on this sample in Fig. 3. According to the test results, each region is found to contain nickel, cobalt, manganese, and

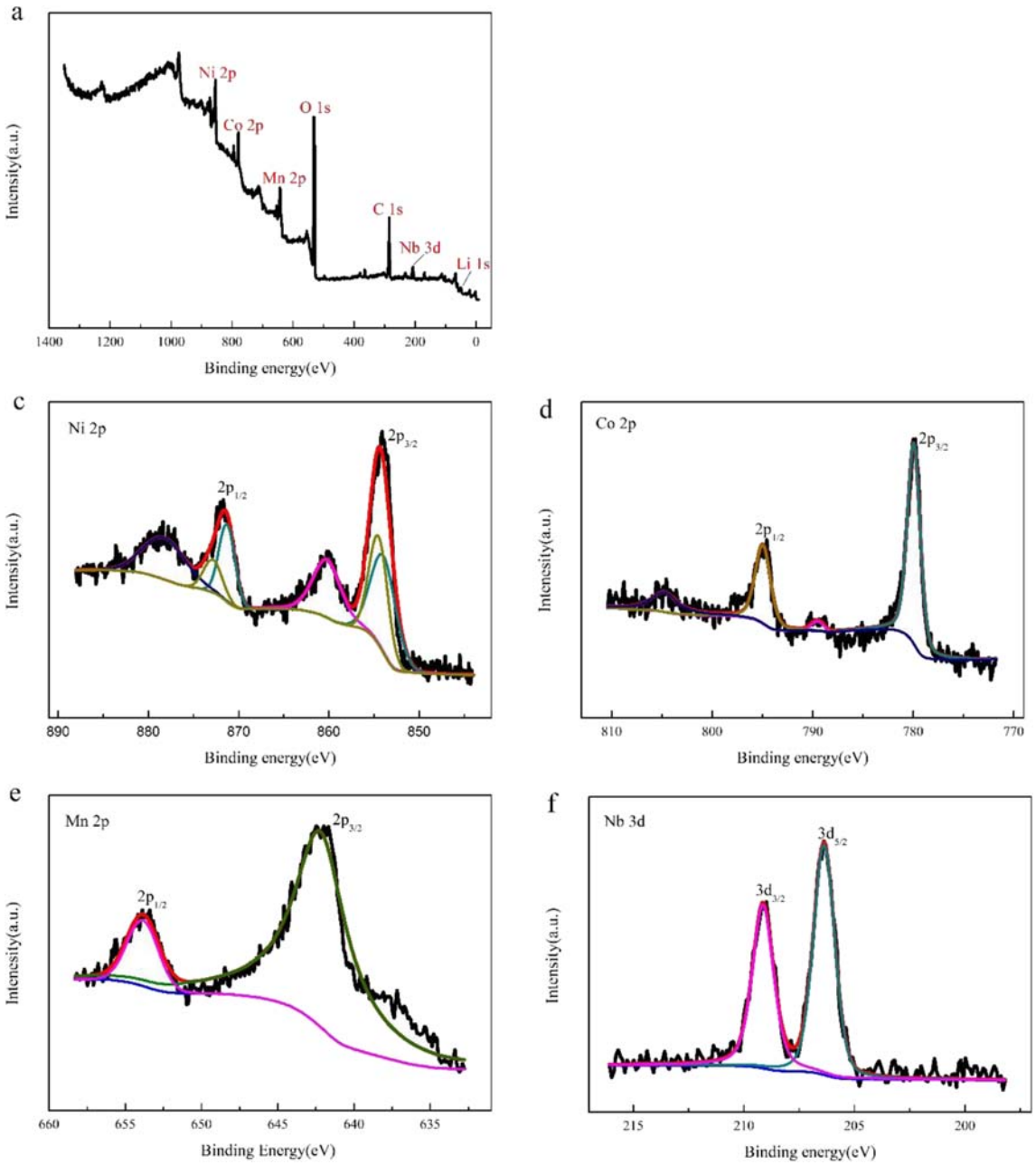

Fig. 4 XPS spectra for Li $(Ni_{0.5}Co_{0.25}Mn_{0.25})_{0.99}Nb_{0.01}O_2$. **a** Full-spectrum. **b** Li 1s. **c** Ni 2p. **d** Co 2p. **e** Mn 2p. **f** Nb 3d

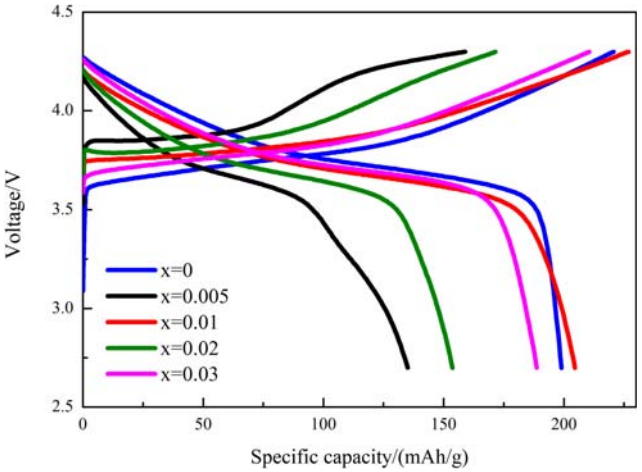

Fig. 5 First charge and discharge curve of Li $(Ni_{0.5}Co_{0.25}Mn_{0.25})_{1-x}Nb_xO_2$

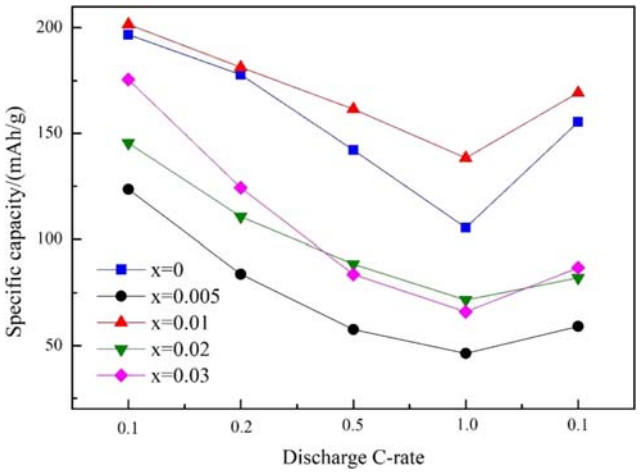

Fig. 7 Average discharge specific capacity curve of Li $(Ni_{0.5}Co_{0.25}Mn_{0.25})_{1-x}Nb_xO_2$

niobium. The relative content of the elements in these two regions is approximately the same, and the atomic percentage ratio is very close to the target chemical formula. It is also proved that Nb^{5+} was successfully doped.

XPS was used to detect the chemical state of various elements on the surface. All spectra were calibrated by assigning the C 1s peak at 284.6 eV. Background type was Shirley. Figure 4a is the binding energy spectrum of Li $(Ni_{0.5}Co_{0.25}Mn_{0.25})_{0.99}Nb_{0.01}O_2$, and Ni 2p, Co 2p, Mn 2p, O 1s, C 1s, Nb 3d, and Li 1s peaks can be observed from it. The C 1s are mainly due to adventitious carbon formed during the atmospheric exposure [29]. The XPS spectrum of Ni 2p has two main peaks and two satellite peaks. The two main peaks are at the peaks of 854.9 eV and 872.4 eV, which are attributed to $2p_{3/2}$ and $2p_{1/2}$. According to the fitted XPS data, Ni $2p_{1/2}$ and Ni $2p_{3/2}$ both contain two splitting peaks corresponding to two different oxidation states of + 2 and + 3 [30, 31], respectively. In Fig. 4d, the two main peaks of the Co 2p spectrum are Co $2p_{3/2}$ at 780.0 eV and Co $2p_{1/2}$ at 794.9 eV, indicating that Co exists mainly in the oxidation state of Co^{3+} [32, 33]. There are two main peaks in the Mn XPS spectrum as shown in Fig. 4e. They are Mn $2p_{3/2}$ at 642.4 eV and Mn $2p_{1/2}$ at 653.9 eV, which are related to Mn^{4+} for the sample. In Fig. 4f, the satellite peaks of Nb appear at 206.4 eV and 209.2 eV corresponding to $3d_{5/2}$ and $3d_{3/2}$, respectively. Consistent with previous literature reports [34, 35], it was proved that Nb^{5+} was successfully doped.

Electrochemical performance

In order to evaluate the electrochemical properties of the material, Fig. 5 shows the initial charge-discharge curve of Li $(Ni_{0.5}Co_{0.25}Mn_{0.25})_{1-x}Nb_xO_2$ ($x = 0$, 0.005, 0.01, 0.02, 0.03) for each material in the range of 2.7–4.3 V at a rate of 0.1C. All the curves in the figure have a charging or discharging platform, and the charging and discharging curves reflect the reversibility of Li insertion/extraction in Li $(Ni_{0.5}Co_{0.25}Mn_{0.25})_{1-x}Nb_xO_2$ crystals during electrochemical process [36]. The generation of the charging or discharging platform in the curve is due to the phase change. If the platform lasts longer, we will

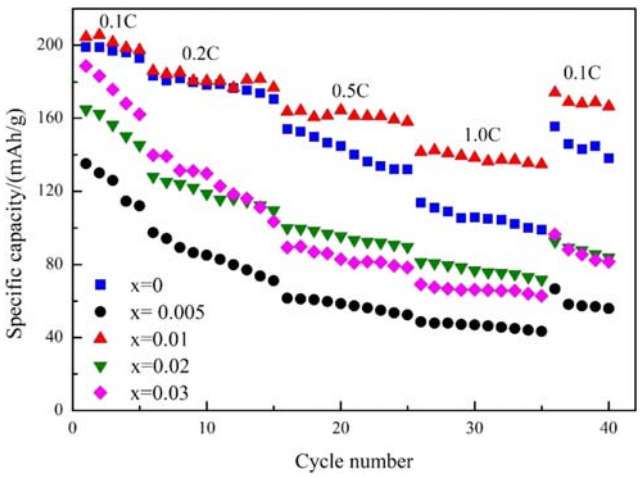

Fig. 6 Rate performance of Li $(Ni_{0.5}Co_{0.25}Mn_{0.25})_{1-x}Nb_xO_2$

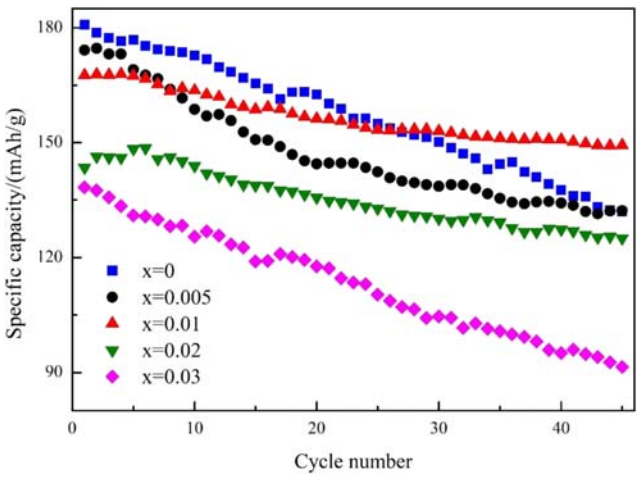

Fig. 8 Cycle performance of Li $(Ni_{0.5}Co_{0.25}Mn_{0.25})_{1-x}Nb_xO_2$

Table 2 Cycle performance analysis of Li $(Ni_{0.5}Co_{0.25}Mn_{0.25})_{1-x}Nb_xO_2$

x	Initial specific charge capacity (mAh/g)	Specific discharge capacity at the 45th cycle (mAh/g)	Capacity retention (%)
$x = 0$	180.8	131.9	72.95
$x = 0.005$	174.1	132.2	75.93
$x = 0.01$	167.6	149.3	89.08
$x = 0.02$	143.4	125.0	87.17
$x = 0.03$	138.3	91.5	66.16

find that the voltage changes more slowly. This results in a higher charge/discharge specific capacity. Due to the precipitation/dissolution of lithium on the electrode surface during charge and discharge, the surface state of the electrode changes and the polarization changes at the same time. This result may make the battery's first charge-discharge curve not smooth [37]. It can be seen from Fig. 5 that when $x = 0$, 0.005, 0.01, 0.02, 0.03, the first discharge specific capacities are 199.0, 135.1, 204.6, 164.7, 188.7 mAh/g, respectively. When $x = 0.01$, the material has the largest initial discharge specific capacity. This indicates that an appropriate amount of Nb^{5+} doping can increase the discharge specific capacity of the original material. This may be due to the fact that an appropriate amount of Nb^{5+} doping can increase the layer spacing and increase the diffusion capacity of Li^+. However, as the amount of Nb^{5+} doping continues to increase, this may result in a decrease in the first discharge specific capacity due to a decrease in the content of the active material Ni^{2+}/Ni^{3+}.

Figure 6 shows the rate performance of materials, and Fig. 7 shows the average specific discharge capacity of the materials at different discharge rates. Each battery is charged to 4.3 V at 0.1C each time, and then discharged to 2.7 V at 0.1C, 0.2C, 0.5C, 1.0C. It can be seen from Figs. 6 and 7 that the discharge specific capacities of different samples at the same discharge rate and the same sample at different discharge

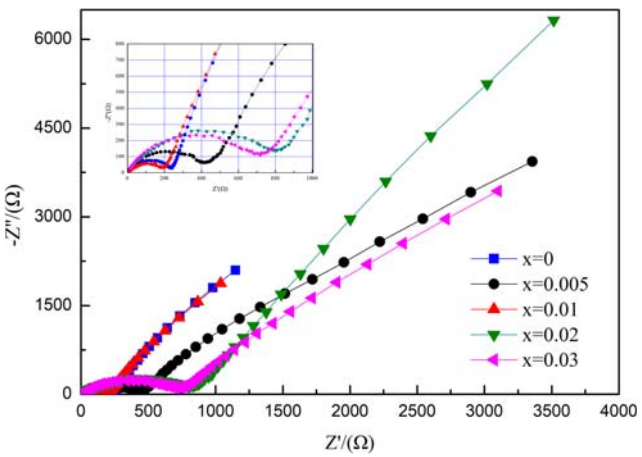

Fig. 9 Electrochemical impedance spectroscopy (EIS) of Li $(Ni_{0.5}Co_{0.25}Mn_{0.25})_{1-x}Nb_xO_2$

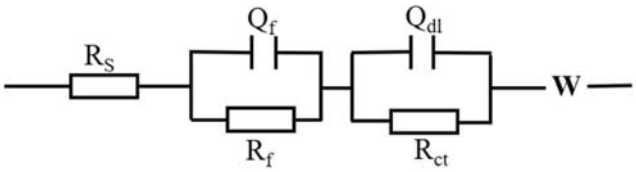

Fig. 10 Electrochemical impedance spectroscopy fitting circuit diagram

rates are significantly different. The former is due to the difference in the electrochemical properties of the material due to the different content of doped Nb^{5+}. In the latter case, the polarization increases as the discharge rate increases. For detailed analysis, the specific discharge capacities of the original materials at 0.1C, 0.2C, 0.5C, 1.0C, and 0.1C are 199.0, 183.3, 154.0, 113.7, and 155.4 mAh/g, respectively. And its average discharge capacities are 196.72, 177.84, 142.16, 105.48, and 155.4 mAh/g, respectively. However, when $x = 0.01$, the discharge specific capacities of the material are 204.6, 186.0, 163.5, 141.6, and 174.1 mAh/g, respectively. And the corresponding average discharge specific capacities are 201.62, 181.34, 161.43, 138.36, and 169.2 mAh/g, respectively. Therefore, the sample Li $(Ni_{0.5}Co_{0.25}Mn_{0.25})_{0.99}Nb_{0.01}O_2$ has the best rate performance. This result may be due to the proper amount of Nb^{5+} doped material, the better insertion/extraction reversibility of Li^+ [25], thereby increasing the reversibility of lithium-ion transfer between the two electrodes [38].

Figure 8 shows the cycle performance of materials for charging and discharging at 2.7–4.3 V at a rate of 0.1C. The cycle performance analysis of the material is shown in Table 2. The capacity retention rate of the original material is 72.95%. When $x = 0.005$, $x = 0.01$, $x = 0.02$, $x = 0.03$ capacity retention rates were 75.93%, 89.08%, 87.17%, and 66.16%, respectively. It is apparent that the capacity retention of the original material is low due to surface structure changes of the active material and decomposition of the electrolyte, which is induced by highly reactive Ni^{4+} and/or some Li residues [5, 39]. The capacity retention of the material is

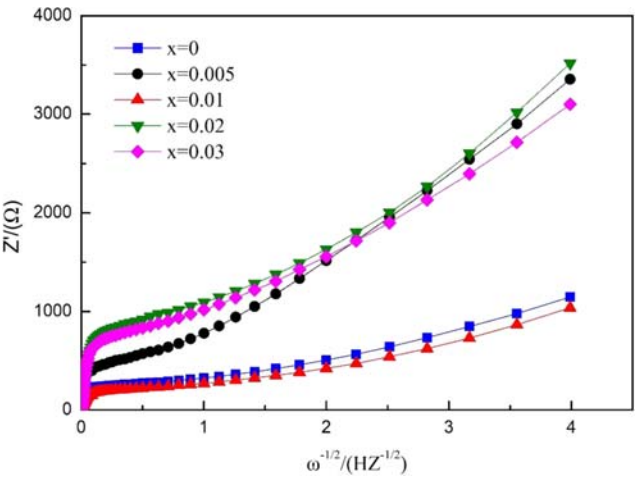

Fig. 11 Linear fitting relationship between Z′and $\omega^{-1/2}$ of Li $(Ni_{0.5}Co_{0.25}Mn_{0.25})_{1-x}Nb_xO_2$

Table 3 EIS fitting data of Li $(Ni_{0.5}Co_{0.25}Mn_{0.25})_{1-x}Nb_xO_2$

Samples	R_s/Ω	R_f/Ω	Q_f/(F)	R_{ct}/Ω	Q_{dl}/(F)	$W/(\Omega \cdot s^{-1/2})$	$D_{Li+}/cm^2\ s^{-1}$
$x = 0$	3.350×10^{-7}	3.2×10^{2}	2.513×10^{-3}	2.4335×10^{2}	1.176×10^{-5}	2.36×10^{-2}	2.330×10^{-14}
$x = 0.005$	1.711×10^{0}	1.455×10^{4}	1.634×10^{-3}	4.242×10^{2}	8.164×10^{-6}	5.776×10^{-5}	4.223×10^{-15}
$x = 0.01$	5.001×10^{1}	9.021×10^{3}	5.292×10^{-3}	2.078×10^{2}	9.665×10^{-5}	4.356×10^{-2}	2.952×10^{-14}
$x = 0.02$	3.795×10^{-5}	8.472×10^{2}	1.990×10^{-5}	3.079×10^{4}	1.790×10^{-3}	5.474×10^{-3}	4.016×10^{-15}
$x = 0.03$	1.257×10^{1}	9.817×10^{3}	3.054×10^{-3}	6.888×10^{2}	1.001×10^{-5}	2.948×10^{-3}	$4.485 \times 10,^{-15}$

improved when the proper amount of Nb^{5+} is doped, and the cycle stability of the material is best when $x = 0.01$. This may be because the bond energy of Nb-O is stronger than that of MO (M = Ni, Co, Mn), and an appropriate amount of Nb doping can stabilize the bulk structure of the cathode material during Li^+-ion intercalation/deintercalation [40].

Figure 9 is a cyclic Nyquist diagram of the electrode, and Fig. 10 is an equivalent circuit diagram. It is clear that the Nyquist plots have similar shapes. The pattern consists of a small intercept, a semicircle in the high frequency region, and a straight line in the low frequency region. They are attributed to the ohmic resistance (R_s) determined by the resistance of the electrolyte and the electrode, the resistance (R_f) of the solid electrolyte interface ((SEI) film) layer, the charge transfer resistance (R_{ct}) at the electrode/electrolyte interface, and Warburg impedance of Li^+ diffusion, respectively [41–43].

The values of the impedance parameters of Table 3 were obtained by fitting the ZSimpWin software, in which the diffusion coefficient (D_{Li+}) of lithium ions in the cathode can be calculated by the following formula [44]:

$$D_{Li+} = R^2T^2/2A^2n^4F^4C^2\sigma^2. \quad (1)$$

$$Z' = k + \sigma\omega^{-1/2}. \quad (2)$$

In Eq. 2, k represents a constant, and σ represents the Warburg factor opposite to Z'. Therefore, to obtain the slope σ, only a function graph of Z' and $\omega^{-1/2}$ is drawn (Fig. 11). In Eq. 1, n is the number of electrons required per unit reaction, R is the gas constant, T is the absolute temperature, n is the number of electrons required to participate in the unit reaction, F is the Faraday constant, A is the area of the cathode/electrolyte interface, and C is the concentration of lithium ions [45, 46].

By comparing the diffusion coefficients (D_{Li+}) of lithium ions of various samples by Table 3, it was found that the original material is lower than Li $(Ni_{0.5}Co_{0.25}Mn_{0.25})_{0.99}Nb_{0.01}O_2$, which were 2.3301×10^{-14} and 2.9515×10^{-14}, respectively. The results show that doping Nb^{5+} can enlarge the interplanar spacing and promote the diffusion of lithium ions, which improves the rate performance and cycle stability of the electrode materials.

Figure 12 is a cyclic voltammogram of the material with a scan voltage of 2.7–4.5 V and a scan rate of 0.1 mV/s. As shown, all materials have only a pair of redox peaks, and no phase transition from the hexagonal phase to the spinel phase occurs during Li-ion intercalation/deintercalation [47]. The oxidation peak on the corresponding curve during charging is related to the oxidation which is related to the oxidation of Ni^{2+}/Ni^{3+} to Ni^{4+} and the oxidation of Co^{3+} to Co^{4+}, indicating that Li^+ is detached from the compound Li $(Ni_{0.5}Co_{0.25}Mn_{0.25})_{1-x}Nb_xO_2$. Upon discharge, a similar reduction peak which corresponds to a decrease in Ni-ions ($Ni^{4+} \rightarrow Ni^{2+}/Ni^{3+}$) and Co-ions ($Co^{4+} \rightarrow Co^{3+}$) indicated in the reverse lithium intercalation layered structure was found. Mn^{4+} is inactive in the structure of Li $(Ni_{0.5}Co_{0.25}Mn_{0.25})_{1-x}Nb_xO_2$ because the valence is 4 [34]. When $x = 0$, 0.005, 0.01, 0.02, 0.03, the oxidation potential peaks were 3.9427 V, 3.9903 V, 3.8281 V, 3.8613 V, 3.9771 V, respectively; the reduction potential peaks were 3.6223 V, 3.6256 V, 3.6410 V, 3.6072 V, 3.6062 V, respectively; the peak difference between the two peaks are 0.3204 V, 0.3647 V, 0.1871 V, 0.2541 V, 0.3709 V, respectively. The peak difference is smaller, which indicates that the polarization of the material is smaller. Therefore, the reversibility of the material during charging and discharging is higher, and the electrochemical performance is better [48]. When the Nb^{5+} doping amount is $x = 0.01$, the minimum potential difference is 0.1871 V, which is smaller than the potential difference of the original material. Thus, an appropriate amount of Nb^{5+} doping reduces the

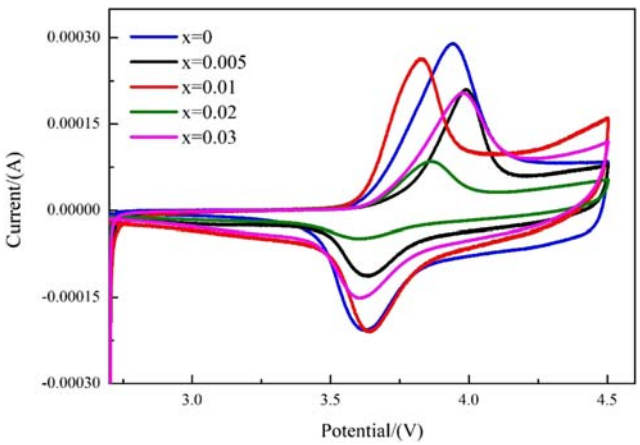

Fig. 12 Cyclic voltammogram of Li $(Ni_{0.5}Co_{0.25}Mn_{0.25})_{1-x}Nb_xO_2$

electrochemical polarization of the original material [49]. Therefore, the material Li $(Ni_{0.5}Co_{0.25}Mn_{0.25})_{0.99}Nb_{0.01}O_2$ has better electrochemical performance, which is consistent with the cycle performance and EIS analysis results.

Conclusion

In this paper, the material Li $(Ni_{0.5}Co_{0.25}Mn_{0.25})_{1-x}Nb_xO_2$ ($x = 0$, 0.005, 0.01, 0.02, 0.03) was synthesized by co-precipitation method, and the materials were structurally analyzed and electrochemically tested. Electrochemical data show that the material Li $(Ni_{0.5}Co_{0.25}Mn_{0.25})_{0.99}Nb_{0.01}O_2$ has the best rate performance, and the specific discharge capacities at 0.1C, 0.2C, 0.5C, and 1C are 204.6, 186.0, 163.5, 141.6 mAh/g, respectively. From 1C to 0.1C, a discharge specific capacity of 174.1 mAh/g is still obtained. And after circulating 45 times at 0.1C, the capacity retention rate is the highest, which is 89.08%. The results show that an appropriate amount of Nb^{5+} doping can reduce the mixing of Li^+/Ni^{2+} and increase the interlayer spacing. Furthermore, the cycle performance and rate performance of the material $LiNi_{0.5}Co_{0.25}Mn_{0.25}O_2$ are improved.

References

1. Li Y-C, Zhao W-M, Xiang W et al (2018) Promoting the electrochemical performance of $LiNi_{0.8}Co_{0.1}Mn_{0.1}O_2$ cathode via $LaAlO_3$ coating. J Alloys Compd 766:546–555
2. Zubi G, Dufo-López R, Carvalho M et al (2018) The lithium-ion battery: state of the art and future perspectives. Renew Sust Energ Rev 89:292–308
3. Liang C, Longo RC, Kong F et al (2017) Obstacles toward unity efficiency of $LiNi_{1-2x}Co_xMn_xO_2$ (x = 0 ~ 1/3) (NCM) cathode materials: insights from ab initio calculations. J Power Sources 340:217–228
4. Da Silva SP, Sita LE, Dos Santos CS et al (2018) Physical and chemical characterization of $LiCoO_2$ cathode material extracted from commercial cell phone batteries with low and high states of health. Mater Chem Phys 213:198–207
5. Ding Y, Mu D, Wu B et al (2017) Recent progresses on nickel-rich layered oxide positive electrode materials used in lithium-ion batteries for electric vehicles. Appl Energy 195:586–599
6. Oz E, Altin S, Demirel S et al (2016) Electrochemical effects and magnetic properties of B substituted $LiCoO_2$: improving Li-battery performance. J Alloys Compd 657:835–847
7. Evertz M, Horsthemke F, Kasnatscheew J et al (2016) Unraveling transition metal dissolution of $Li_{1.04}Ni_{1/3}Co_{1/3}Mn_{1/3}O_2$ (NCM 111) in lithium ion full cells by using the total reflection X-ray fluorescence technique. J Power Sources 329:364–371
8. Lars R, Jinlong L, Björn S et al (2016) Effect of pristine nanostructure on first cycle electrochemical characteristics of lithium-rich lithium–nickel–cobalt–manganese-oxide cathode ceramics for lithium ion batteries. J Power Sources 306:135–147
9. Liang C, Kong F, Longo RC et al (2016) Unraveling the origin of instability in Ni-rich $LiNi_{1-2x}Co_xMn_xO_2$ (NCM) cathode materials. Am Chem Soc 120:6383–6393
10. Zhang Q, Su Y, Chen L et al (2018) Pre-oxidizing the precursors of nickel-rich cathode materials to regulate their Li^+/Ni^{2+} cation ordering towards cyclability improvements. J Power Sources 396:734–741
11. Yan P, Zheng J, Lv D et al (2015) Atomic-resolution visualization of distinctive chemical mixing behavior of Ni, Co, and Mn with Li in layered lithium transition-metal oxide cathode materials. Am Chem Soc 27:5393–5401
12. Xu C, Xiang W, Wu Z, Xu Y, Li Y, Wang Y, Xiao Y, Guo X, Zhong B (2019) Highly stabilized Ni-rich cathode material with Mo induced epitaxially grown nanostructured hybrid surface for high-performance lithium-ion batteries. ACS Appl Mater Interfaces 11: 16629–16638
13. Zhang G, Qiu B, Xia Y et al (2019) Double-helix-superstructure aqueous binder to boost excellent electrochemical performance in Li-rich layered oxide cathode. J Power Sources 420:29–37
14. Ahmed S, Pokle A, Schweidler S et al (2019) The role of intragranular nanopores in capacity fade of nickel-rich layered Li $(Ni_{1-x-y}Co_xMn_y)O_2$ cathode materials. ACS Nano:10694–10704
15. Sim S-J, Lee S-H, Jin B-S et al (2019) Improving the electrochemical performances using a V-doped Ni-rich NCM cathode. Sci Rep 9:8952
16. Ke X, Wang Y, Ren G et al. (2019) Towards rationally mechanical design of inorganic solid electrolytes for all-solid-state lithium ion batteries. Energy Storage Materials
17. Qiu L, Xiang W, Tian W et al (2019) Polyanion and cation co-doping stabilized Ni-rich Ni–Co–Al material as cathode with enhanced electrochemical performance for Li-ion battery. Nano Energy 63:103818
18. Sun L, Zhu L, Mi C et al (2019) The effects of Cr substitution on $LiNi_{0.65}Co_{0.1}Mn_{0.25}O_2$ for lithium-ion batteries. Ionics 25: 3021–3030
19. Mi C, Han E, Li L et al (2018) Effect of iron doping on $LiNi_{0.35}Co_{0.30}Mn_{0.35}O_2$. Solid State Ionics 325:24–29
20. Lu M, Han E, Zhu L et al (2016) The effects of Ti^{4+}-Fe^{3+} co-doping on Li $[Ni_{1/3}Co_{1/3}Mn_{1/3}]O_2$. Solid State Ionics 298:9–14
21. Liu X-H, Kou L-Q, Shi T et al (2014) Excellent high rate capability and high voltage cycling stability of Y_2O_3-coated $LiNi_{0.5}Co_{0.2}Mn_{0.3}O_2$. J Power Sources 267:874–880
22. Li L, Zhang Z, Fu S et al (2018) Co-modification by $LiAlO_2$-coating and Al-doping for $LiNi_{0.5}Co_{0.2}Mn_{0.3}O_2$ as a high-performance cathode material for lithium-ion batteries with a high cutoff voltage. J Alloys Compd 768:582–590
23. Yoo G-W, Jang B-C, Son J-T (2015) Novel design of core shell structure by NCA modification on NCM cathode material to enhance capacity and cycle life for lithium secondary battery. Ceram Int 41:1913–1916
24. Wua J, Liu H, Ye X et al (2015) Effect of Nb doping on electrochemical properties of $LiNi_{1/3}Co_{1/3}Mn_{1/3}O_2$ at high cutoff voltage for lithium-ion battery. J Alloys Compd 644:223–227
25. Hu X, Guo H, Peng W et al (2018) Effects of Nb doping on the performance of $0.5Li_2MnO_3 \cdot 0.5LiNi_{1/3}Co_{1/3}Mn_{1/3}O_2$ cathode material for lithium-ion batteries. J Electroanal Chem 822:75–65
26. Yi T-F, Yin L-C, Ma Y-Q et al (2013) Lithium-ion insertion kinetics of Nb-doped $LiMn_2O_4$ positive-electrode material. Ceram Int 39: 4673–4678
27. Lei T, Li Y, Su Q et al (2018) High-voltage electrochemical performance of $LiNi_{0.5}Co_{0.2}Mn_{0.3}O_2$ cathode materials via Al concentration gradient modification. Ceram Int 44:8809–8817
28. Liu H, Han E, Li L et al (2019) Effect of Cu^{2+} on Li $[Li_{0.2}Ni_{0.2}Co_{0.08}Mn_{0.52}]O_2$ at different stages. Ionics 25: 3009–3020
29. Xu Y-D, Xiang W, Wu Z-G et al (2018) Improving cycling performance and rate capability of Ni-rich $LiNi_{0.8}Co_{0.1}Mn_{0.1}O_2$ cathode materials by $Li_4Ti_5O_{12}$ coating. Electrochim Acta 268:358–365

30. Huang D, Shi Y, Tornheim AP et al (2019) Nanoscale $LiNi_{0.5}Co_{0.2}Mn_{0.3}O_2$ cathode materials for lithium ion batteries via a polymer-assisted chemical solution method. Appl Mater Today 16:342–350
31. Park S, Kim D, Ku H et al (2019) The effect of Fe as an impurity element for sustainable resynthesis of Li $[Ni_{1/3}Co_{1/3}Mn_{1/3}]O_2$ cathode material from spent lithium-ion batteries. Electrochim Acta 296:814–822
32. Jo M, Park S, Song J et al (2018) Incorporation of Cu into Li $[Ni_{1/3}Co_{1/3}Mn_{1/3}]O_2$ cathode: elucidating its electrochemical properties and stability. J Alloys Compd 764:112–121
33. Zhang J, Cao Y, Ou X et al (2019) Constituting the NASICON type solid electrolyte coated material forming anti-high voltage system to enhance the high cut-off voltage performance of $LiNi_{0.6}Co_{0.2}Mn_{0.2}O_2$ via charge attracts electrostatic assembly. J Power Sources 436:226722
34. Yang Z, Xiang W, Wu Z et al (2017) Effect of niobium doping on the structure and electrochemical performance of $LiNi_{0.5}Co_{0.2}Mn_{0.3}O_2$ cathode materials for lithium ion batteries. Ceram Int 43:3866–3872
35. Lv C, Yang J, Peng Y et al (2019) 1D Nb-doped $LiNi_{1/3}Co_{1/3}Mn_{1/3}O_2$ nanostructures as excellent cathodes for Li-ion battery. Electrochim Acta 297:258–266
36. Tsai H-L, Hsieh C-T, Li J et al (2018) Enabling high rate charge and discharge capability, low internal resistance, and excellent cycleability for Li-ion batteries utilizing graphene additives. Electrochim Acta 273:200–207
37. Ivanishchev AV, Bobrikov IA, Ivanishcheva IA et al (2018) Study of structural and electrochemical characteristics of $LiNi_{0.33}Mn_{0.33}Co_{0.33}O_2$ electrode at lithium content variation. J Electroanal Chem 821:140–151
38. Huang Z, Wang Z, Jing Q et al (2016) Investigation on the effect of Na doping on structure and Li-ion kinetics of layered $LiNi_{0.6}Co_{0.2}Mn_{0.2}O_2$ cathode material. Electrochim Acta 192:120–126
39. Yao X, Xu Z, Yao Z et al (2019) Oxalate co-precipitation synthesis of $LiNi_{0.6}Co_{0.2}Mn_{0.2}O_2$ for low-cost and high-energy lithium-ion batteries. Mater Today Commun 19:262–270
40. Lv C, Peng Y, Yang J et al (2018) Electrospun Nb-doped $LiNi_{0.4}Co_{0.2}Mn_{0.4}O_2$ nanobelts for lithium ion battery. Inorg Chem Front
41. Ding X, Li Y-X, Deng M-M et al (2019) Cesium doping to improve the electrochemical performance of layered $Li_{1.2}Ni_{0.13}Co_{0.13}Mn_{0.54}O_2$ cathode material. J Alloys Compd 791:100–108
42. Mi C, Han E, Sun L et al (2019) Effect of Ti^{4+} doping on $LiNi_{0.35}Co_{0.27}Mn_{0.35}Fe_{0.03}O_2$. Solid State Ionics 340:114976
43. Huang J, Fang X, Wu Y et al (2018) Enhanced electrochemical performance of $LiNi_{0.8}Co_{0.1}Mn_{0.1}O_2$ by surface modification with lithium-active MoO_3. J Electroanal Chem 823:359–367
44. Xu C-L, Xiang W, Wu Z-G et al (2018) A comparative study of crystalline and amorphous $Li_{0.5}La_{0.5}TiO_3$ as surface coating layers to enhance the electrochemical performance of $LiNi_{0.815}Co_{0.15}Al_{0.035}O_2$ cathode. J Alloys Compd 740:428–435
45. Dong T, Peng P, Jiang F (2018) Numerical modeling and analysis of the thermal behavior of NCM lithium-ion batteries subjected to very high C-rate discharge/charge operations. Int J Heat Mass Transf 117:261–272
46. Zhao W, Luo G, Wang C-Y (2015) Modeling internal shorting process in large-format Li-ion cells. J Electrochem Soc 162: A1352–A1364
47. Ryu W-H, Lim S-J, Kim W-K et al (2014) 3-D dumbbell-like $LiNi_{1/3}Mn_{1/3}Co_{1/3}O_2$ cathode materials assembled with nano-building blocks for lithium-ion batteries. J Power Sources 257: 186–191
48. Han E, Du X, Yang P et al (2017) The effects of copper and titanium co-substitution on $LiNi_{0.6}Co_{0.15}Mn_{0.25}O_2$ for lithium ion batteries. Ionics 24:393–401
49. Jia X, Yan M, Zhou Z et al (2017) Nd-doped $LiNi_{0.5}Co_{0.2}Mn_{0.3}O_2$ as a cathode material for better rate capability in high voltage cycling of Li-ion batteries. Electrochim Acta 254:50–58